Battery-Aware Operation Range Estimation for Terrestrial and Aerial Electric Vehicles

Battery-Aware Operation Range Estimation for Terrestrial and Aerial Electric Vehicles

Donkyu Baek, *Member, IEEE*, Yukai Chen, *Member, IEEE*, Alberto Bocca, *Member, IEEE*, Lorenzo Bottaccioli, *Member, IEEE*, Santa Di Cataldo, *Member, IEEE*, Valentina Gatteschi, *Member, IEEE*, Daniele Jahier Pagliari, *Member, IEEE*, Edoardo Patti, *Member, IEEE*, Gianvito Urgese, *Member, IEEE*, Naehyuck Chang, *Fellow, IEEE* Alberto Macii, *Senior Member, IEEE*, Enrico Macii, *Fellow, IEEE* Paolo Montuschi, *Fellow, IEEE*, Massimo Poncino, *Fellow, IEEE*

***Abstract*—The range of operations of electric vehicles (EVs) is a critical aspect that may affect the user's attitude towards them. For manned EVs, range anxiety is still perceived as a major issue and recent surveys have shown that one third of potential European users are deterred by this problem when considering the move to an EV. Similar consideration applies to aerial EVs for commercial use, where a careful planning of the flying range is essential to guarantee the service but also to avoid the loss of the EVs due to charge depletion during the flight.**

Therefore, route planning for EVs for different purposes (range estimation, route optimization) and/or application scenarios (terrestrial, aerial EVs) is an essential element to foster the acceptance of EVs as a replacement of traditional vehicles.

One essential element to enable such accurate planning is an accurate model of the actual power consumption. While very elaborate models for the electrical motors of EVs do exist, the motor power does not perfectly match the power drawn from the battery because of battery non-idealities.

In this work we propose a general methodology that allows to predict and/or optimize the operation range of EVs, by allowing different accuracy/complexity tradeoffs for the models describing the route, the vehicle and the battery, and taking into account the decoupling between motor and battery power.

We demonstrate our method on two use cases. The first one is a traditional driving range prediction for a terrestrial EV; the second one concerns the energy-optimal delivery scheduling for an unmanned aerial vehicle.

***Keywords*—State of charge, Battery non-ideality, Energy-efficient scheduling, Electric vehicles, Operation range estimation**

This work was supported by the National Research Foundation of Korea (NRF) grant funded by the Korea government (MSIP) (No. NRF-2018R1A2B3007894).

D. Baek, Y. Chen, A. Bocca, S. Cataldo, V. Gatteschi, D. Pagliari, E. Patti, G. Urgese, A. Macii, E. Macii, P. Montuschi, and M. Poncino are with the Department of Control and Computer Engineering, Politecnico di Torino, Italy (e-mail: donkyu.baek@polito.it; yukai.chen@polito.it; alberto.bocca@polito.it; santa.dicataldo@polito.it; valentina.gatteschi@polito.it; daniele.jahier@polito.it; edoardo.patti@polito.it; gianvito.urgese@polito.it; alberto.macii@polito.it; enrico.macii@polito.it; paolo.montuschi@polito.it; massimo.poncino@polito.it).

L. Bottaccioli is with the Energy Center Lab, Politecnico di Torino, Italy (e-mail: lorenzo.bottaccioli@polito.it).

N. Chang is with the School of Electrical Engineering, Korea Advanced Institute of Science and Technology (e-mail: naehyuck@cad4x.kaist.ac.kr).

I. Introduction

In the last few years, electric vehicles (EVs) have shifted from absolute novelty to ordinary in most sectors of public and private transportation. The market demand for electric cars is rapidly growing, in addition to small vehicles such as electric hover-boards, skateboards and bikes. Unmanned aerial vehicles (UAVs) or drones are also becoming more and more popular, as a large number of logistics companies such as UPS, DHL and Amazon are heavily investing on drone package delivery. Nonetheless, the reduced energy storage capacity of the batteries translates into range limitation problems for EVs, acting as a barrier to widespread adoption compared to traditional vehicles based on internal combustion engines (ICEs). While accurately predicting the range of operations for ICEs has never been considered a significant problem, because re-fueling is usually fast and readily available but for very peculiar geographical contexts, range prediction for battery-operated vehicles (driving or flying range for terrestrial and aerial vehicles, respectively) is receiving ever-growing attention. The reason of this interest is to be found in the increased diffusion and critical role of EVs in various application domains (personal and commercial transportation, surveillance, etc.) as well as in the technical and logistic difficulties involved with the re-charging.

Compared to traditional ICEs, range estimation prediction is a very challenging multi-factorial problem, involving a large number of variables that are not always easy to estimate. Besides the technical characteristics of the vehicle, for on-road EVs (e.g. electric cars) the factors that need to be taken into account include road topology and grade, speed, acceleration/deceleration patterns, use of the in-board electric devices (e.g. A/C) as well as driving style (e.g. normal vs aggressive). For aerial EVs (e.g. drones), payload and delivery task characteristics (e.g. take-off, flying and landing speeds). On the other hand, additional challenges are posed by maintaining the range estimation computationally light, so that it can be easily executed by on-board computers. To achieve this purpose, some of the aforementioned factors are either simplified or neglected in the standard practice, imposing an accuracy/complexity trade-off.

As a matter of fact, most of the available range estimators over-simplify the problem by considering in their computation the electrical energy/power drawn by the motor, which does

not have a perfect 1:1 match with the energy/power that is actually drawn by the battery. The reason of this mismatch is mainly two-fold: (i) the power delivered by the battery is not constant, as it depends on its current state of charge (SOC). More specifically, the lower the SOC, the lower the efficiency of the battery. Hence, a partially charged battery will be depleted more than a fully-charged one for the same task and under the same conditions. On top of that, the efficiency drop is not linear [1]. (ii) the conversion process that delivers power from the battery to the motor is not ideal. The former aspect is particularly relevant, as it suggests that summing up the energy demands of the intermediate tracts without taking the non-linear relation between the available battery capacity and SOC into account, as it is done by most range estimators, will unavoidably result into inaccurate range predictions.

To address this issue, in this paper we propose a battery-aware methodology, that is suitable for both terrestrial and aerial battery operated vehicles. More specifically, we incorporate the state-dependency characteristics of a state-of-the-art battery into the range estimator and provide an overall methodology to build a model and extract accurate range predictions in a realistic scenario.

We will demonstrate our solution on two use cases relative to different types of vehicles, for which accurate range prediction is especially relevant. The first use case is a traditional driving range prediction for a terrestrial EV, and more specifically a fully electric passenger car. We will show how a traditional battery model over-estimates the actual energy consumption of the car, suggesting a route that is not the most (battery) energy efficient. The second use case concerns an unmanned aerial vehicle. Our method will be used to determine the energy-optimal flying speed for a parcel delivery task in which a number of packages are to be delivered to a set of destinations. Unlike in the former case, flying speed can be considered a free variable for aerial EVs thanks to absence of traffic. Our solution will show that a battery-aware delivery schedule can carry more packages than the traditional delivery model with the same battery capacity.

In the rest of the paper we will use the following non-standard terminology to denote the two categories of EVs addressed in this work: TEVs for terrestrial EVs, and AEVs for aerial ones[1].

The paper is organized as follows. Section II introduces the required background and presents related work. Section III describes the conceptual flow of our proposed method. Section IV presents the details of the battery modeling. Sections V and VI describe implementation and simulation results of the TEV driving range estimation and of the AEV delivery optimization, respectively. Finally, Section VII concludes the paper.

II. Background and Related Work

A high number of research activities are currently devoted to optimize energy efficiency in TEVs and AEVs, as both of them are expected to experience an increasing adoption by the wider public [2]–[4]. Concerning TEVs, as previously mentioned, although estimation of the driving range or mileage for vehicles with internal combustion engine (ICE) motors is generally accurate, this is not the case for fully electric passenger cars. In fact, battery pack capacity (Ah), or electrical energy (kWh), depends largely on factors such as charge/discharge current profile, SOC, temperature, and driving style [5], [6]. In addition, the pack has a continuous slight deterioration over time regarding the total capacity, even in the case of parking the vehicle for a long time.

Hence, several works were recently targeted at improving the estimation of the driving range for TEVs. In [7], the authors propose a model for simulating the change in battery SOC in EVs, along routes during trips. Nonetheless, this model concerns orienteering problems instead of real battery characteristics, when analyzing the energy consumption in a routing trip. In [8], the prediction of SOC is based on an Adaptive Recurrent Neural Network after considering both the route (vehicle speed and terrain profile) and driving style. Although this approach is similar to the one presented in the current work, the battery model is only based on linear characteristics and, therefore, it only partially considers the effect of the current, on the total capacity depletion. The work presented in [9] deals with the prediction of energy consumption based on route information, weather conditions and driving behavior, whereas the research described in [10] relies on real-time information gathered by other vehicles to suggest routes based on traffic information and expected waiting time for battery switching at robot-controlled recharging stations. Also in these cases, the proposed model does not consider that the efficiency of the battery depends on its SOC. As highlighted by the above works, approaches for energy optimization in TEVs generally consider simple battery models based on the nominal energy [11]–[13]. Nonetheless, this approach is in contrast to the real performance of LiPo batteries and the consequent issues [6], [14], especially for the estimation of the battery SOC for which the existing methods differ in complexity and error level [5], [15]–[17].

As in the case of TEVs, also in the context of AEVs' path planning the real performance of the battery is rarely considered. The model proposed in [18] with the aim of determining minimum-energy paths for quadrotors considers the angular acceleration of the propellers, but does not take into account the energy storage properties. In [19], the authors propose an algorithm to minimize the total energy consumption of a quadrotor performing image reconstruction of graphical zones. In this work, the proposed power model characterizes the consumption of the drone operating in different conditions, but does not consider the battery performance. Another work addresses the issue of energy efficient coverage path planning for drones [20]. Nonetheless, the related energy model is based only on empirical measurements during the flights.

Rather than planning a flying path, other works aim at investigating drones' energy consumption under different conditions, by studying the impact of flying maneuvers and velocities on energy consumption [21] or the influence on performance of physical, mechanical, or electrical drones' hardware characteristics [22]. In [23], the performance of different LiPo batteries for drones is analyzed using different models, related to the capacity rate effect. As expected, experimental results show a difference with respect to the data obtained from these models.

[1]We prefer the latter to UAVs as AEVs are not necessarily unmanned.

In [24], an altitude controller based on battery SOC is described. The proposed model relies on the equivalent electrical circuit of [25] applied to LiPo batteries, and the relationship between nominal thrust and battery SOC is provided.
Several works proposed approaches for routing optimization in drone delivery, as in the case of [26]. Nonetheless, the power model presented in [26] only includes the weight of the battery, in addition to payload. The work of [27], instead, proposes a model for minimizing the delivery time for multiple packages. In this case, however, the battery performance is considered just from a service time point of view. Hence, as highlighted by [26], [27], also in the context of drone delivery, authors generally only consider motor power models and possibly a linear characteristic of the energy source, when analyzing the relationship between power consumption, assigned tasks and available battery energy [28], [29]. That is the reason why predictions of the overall flight time are overestimated [30].

III. Methodology

Figure 1 shows the conceptual flow of our methodology for the estimation of the operation range of EVs. Three descriptive sets of data are required as inputs.

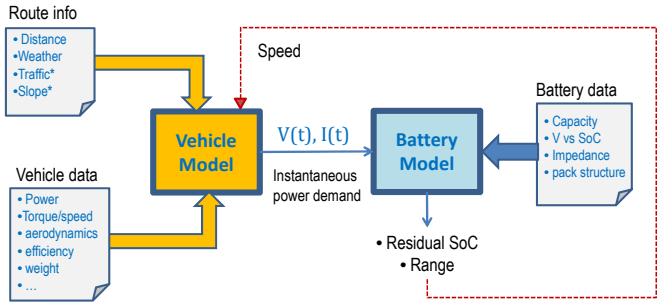

Figure 1. Overall Concept of the Proposed Methodology.

- **Vehicle data**: These information concern the mechanical and electrical characteristics that can affect the power consumption of the vehicle, such as electric motor power, torque/speed characteristics, curb and gross weight, aerodynamic drag, etc. Some of these data depend on the type of vehicle; for instance aerodynamic parameters have different meaning for a terrestrial vehicle (e.g., drag and frontal area) with respect to an aerial one (e.g., wing profile).
- **Route data**: The information about the route to be covered are the ones that differ most depending on the type of vehicle. For TEVs, slope and traffic matter, and can be obtained by pre-processing figures from publicly available services (e.g., [31]).
  An important point is that for TEVs speed is not a free variable and is mostly determined by traffic, road profile and ultimately by speed limits. On the other hand, AEVs do not generally have traffic limitations nor an equivalent of slope; therefore, in this case speed in a free variable. However, it might be possible also for TEVs that the speed could be regulated differently from what the traffic and road conditions would determine (e.g., to increase the driving range).
  To support this option, the diagram shows a "control" loop from the output of the battery model (essentially the residual state of charge) that can be used to tune the speed in the cases when it can override the value determined by the route properties. In one of the use cases analyzed in this paper we will explicitly show ho to use this knob.
  Weather is also another possible variable to be considered, although the way it affects the travel conditions in different ways depending on the type of vehicle.
  Item in the *Route info* box that are listed with a "*" indicate elements that are relevant to TEVs only.
- **Battery Data**: These information concern the battery pack that powers the EV and it is virtually independent of the vehicle type; in fact, what matters is essentially the electrical properties of the individual battery cell, which is then scaled up according to the organization of the battery pack (series/parallel). For this reason, we will elaborate the characteristics and the operations of the battery model in a separate section as they apply to both use cases.

Vehicle and route data are then fed to a model of the vehicle, which will clearly be different for TEVs and AEVs. The model, based on its inputs will output a waveform of the electrical motor power $P(t)$. For a better matching with the characteristics of the battery, we actually decouple power into a pair of voltage and current waveforms $V(t)$ and $I(t)$.
On the other side of the flow, the battery data are used as parameters of a generic battery model; the latter takes then the voltage and current waveforms and yields the evolution of the battery SOC over time and an estimate of the range covered. It is important to mention the the battery model includes the efficiency of the power conversion required to adapt the voltage and current levels requested by the electrical motor and the voltage level of the battery pack. Since voltage levels in particular will not be identical, they need to be adapted via a DC/DC converter, whose efficiency is not ideal.
A nice feature of the proposed flow is that it is allows different accuracy/complexity tradeoffs. By using a standardized representation of the route and of the vehicle data, depending on the available information, the vehicle model will output a more or less accurate power profile. For instance, if traffic info are unavailable, the vehicle speed will be determined by speed limits only; similarly, if some vehicle data are not available, the model will be simplified accordingly. The same consideration applies to the battery model. As battery data will be derived from public specs such as a datasheet, it might be the case that not required data will be available, in which case the model will include only the effects that can be modeled with the quantities at hand.

IV. Battery Modeling

Battery Energy Storage System (BESS) is an important module in an electric vehicle. Therefore, sophisticated battery models play a critical role in the design and optimization of the related

energy processes. For instance, UAV flight time estimation and EV range prediction are possible only through advanced battery models and estimation techniques. In the literature, and according to the various modeling techniques, there are three main categories of battery models: mathematical models, electrochemical models and electrical Equivalent Circuit Models (ECMs). Due to the complexity of the parameter identification and heavy computation for the mathematical and electrochemical models, we adopt an ECM to simulate battery performances. An ECM consists of combining resistors, capacitors, and voltage or current sources. Figure 2 shows a common ECM, which is considered as a sort of standard in the electronic design field thanks to its relatively good compromise between accuracy and simplicity.

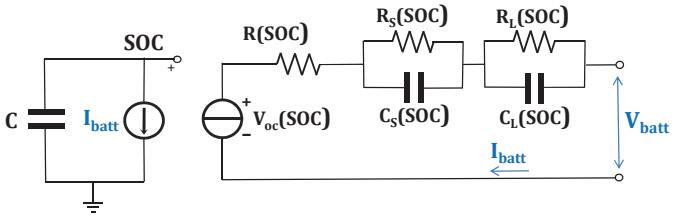

Figure 2. The widely used ECM in electronic design domain [25].

The left part of the ECM in Figure 2 includes a capacitor C representing the nominal capacity, and a current generator modeling the load current I_{batt}. The voltage across the capacitor tracks the SOC of the battery (node SOC). In the right branch, a voltage-controlled generator expresses the non-linear dependence of battery open-circuit voltage V_{oc} on SOC. The RC network models the battery impedance: the series resistance $R(SOC)$ models the internal resistance, whereas the two RC blocks tracking the short-term (R_S, C_S) and long-term (R_L, C_L) time constants of a step response. This model can track the battery voltage V_{batt} over time for load current profiles with different dynamics, even if they have the same average values. However, when it comes to tracking the SOC, it is evident that the constant current generator I_{batt} on the left side will result in same among different load current profiles with same average values as illustrated in [32], which is not the expected behavior since the *Rated Capacity* effect exists inside battery.

Rated Capacity effect is a well-known non ideality of a battery. It indicates that the usable capacity of a battery depends on the magnitude of the discharge current: at larger currents, a battery is less efficient in converting its chemically stored energy into electrical energy. In order to show the *Rated Capacity* effect in the ECM shown in Figure 2, [33] proposed to represent this effect by adding a voltage generator $V_{lost}(I_{load})$ in series to the left part of the model (see Figure 3) that reduces the available charge of the battery by considering the real-time load current values. With this addition, SOC is affected in a more pronounced way by a larger current than for a smaller one. Although this ECM is more accurate for SOC tracking, it cannot distinguish between two current square-wave loads with the same average and swing values but different frequencies. It is intuitive that a higher frequency load stresses the battery more, as the electrochemical reactions occur at a higher frequency. This dependency on load frequency is somehow underrated; however, this effect is not negligible as revealed in [32]. For this reason, another ECM is proposed, as shown in Figure 3, where the load frequency dependence is modeled by adding the voltage generator $V_{lost}(f_{load})$ on the left side of the circuit.

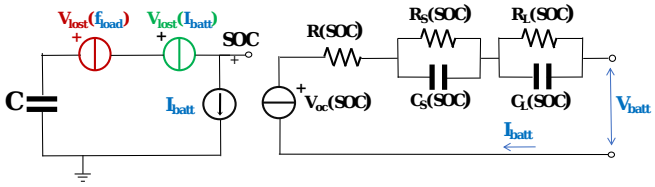

Figure 3. The ECM accounting for load current magnitude and frequency [32].

In this paper, we adopt the ECM in Figure 3 for battery energy analysis. The basic electrical parameters in Figure 2 can be extracted from battery manufacture data-sheets through the methods described in [34]. For a given battery, the methodologies to derive the dependence of battery capacity on current load magnitude and frequency, that is represented by the two voltage generators on the left side of the ECM in Figure 3, are introduced in [35]. The instruction of how to use the model at run-time, in particular for what concerns the frequency-dependent behavior, are illustrated in [32].

Notice that Figure 3 shows the ECM for one single battery cell. However, a BESS installed in terrestrial electric vehicles is always a battery pack that is composed of a large number of cells connected in series and parallel configurations. Concerning the battery pack modeling, we follow the commonly used approach that assuming all the cells behave identically within the pack. Therefore, in this work we implement an ideal scaling of the battery cell ECM according to the serial and parallel connectivity of the cells, for a faster simulation and a higher flexibility in modeling large battery packs. For this purpose, the model components (SOC/OCV characteristic, series resistance, nominal capacity) of the cell model are scaled-up ideally according to the serial and parallel interconnection of the battery cells in a pack. In this way, not all the cells have to be simulated individually.

V. Use Case 1: Driving Range Estimation for TEVs

A. TEV Model

Power consumption of an EV is affected by the body shape, weight, road slope and tires as well as the vehicle speed and acceleration because of vehicle dynamics. There are four resistances acting on a vehicle: rolling resistance F_R, gradient resistance F_G, inertia resistance F_I, and aerodynamic resistance F_A. The power consumption at the EV powertrain

against the resistances is:

$$P_{dyna} = F\frac{ds}{dt} = Fv = (F_R + F_G + F_I + F_A)v$$
$$F_R \propto C_{rr}W,\ F_G \propto W sin\theta,\ F_I \propto ma,\ F_A \propto \frac{1}{2}\rho C_d A v^2$$
$$P_{dyna} \approx (\alpha + \beta sin\theta + \gamma a + \delta v^2)mv \tag{1}$$

C_{rr}, W, θ, m, v, a, C_d, A are rolling coefficient, weight, road slope, vehicle mass, speed, acceleration, drag coefficient and vehicle facial area, respectively. This equation can be simplified as a function of 4 coefficients α, β, γ and δ.

The efficiency of the powertrain (electric motor and drivetrain) depends on the RPM (revolutions per minute) and torque, as well as on the mechanical movement of the drivetrain while delivering power to the wheels. The following EV power model considers these losses [11].

$$P_{EV} = P_{dyna} + C_0 + C_1 v + C_2 v^2 + C_3 T^2 \tag{2}$$

where C_0, C_1, C_2, and C_3 are the coefficients for constant loss, iron and friction loss, drivetrain loss and copper loss.

EVs leverage regenerative braking to convert kinetic energy to electric energy during deceleration. The power generated by regenerative braking is modeled as a function of the negative motor torque and vehicle speed.

$$P_{regen} = \epsilon T v + \zeta \tag{3}$$

where ϵ and ζ are regenerative braking coefficients.

Advanced vehicle simulators are very accurate in estimating powertrain consumption [36]. However, they are not suitable for on-board range estimation due to their significant runtime overheads. Thus, we use the simpler power model expressed by (1), (2) and (3). Model coefficients are extracted from a single offline vehicle simulation. The validation of the model and its parameter extraction are discussed in Section V-C1.

B. Route Model

We model routes as an array of *segments*, each representing a portion of road with a unique speed and slope. Speed limits and road traffic are used to determine speed, whereas road slopes are obtained from altitude profiles. These information are extracted from Google Maps APIs [31], as shown in Figure 4 for an example route. Each color on the route corresponds to a different level of traffic, as shown in the legend.

Figure 5 shows the translation of the raw data of Figure 4 into a list of segments. The top plot shows the speed limits contained in the road metadata. The second plot shows the levels of traffic along the route, while the third one the actual speed considering traffic. The fourth plot shows the slopes of the route: the red line is the slope directly obtained from the altitude data of Figure 4, whereas the blue line is the result of a discretization process. Such process is needed to avoid having a huge number of extremely small segments. Specifically, we do not consider slope changes smaller than 5% of the maximum altitude variation of the route. Segments are then determined in correspondence of any speed or slope

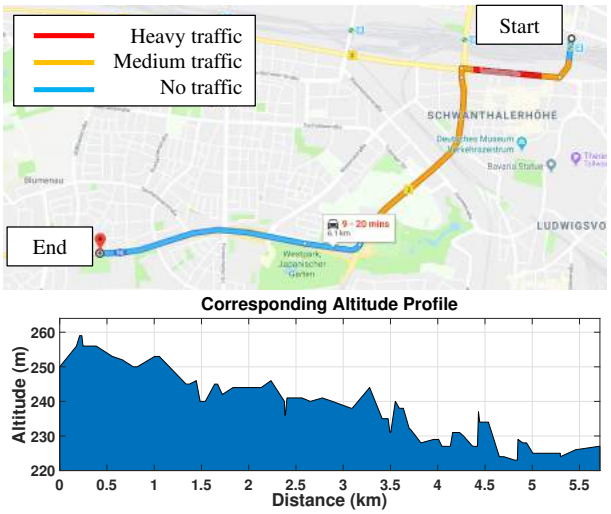

Figure 4. An example route and corresponding altitude profile on Google Maps [31].

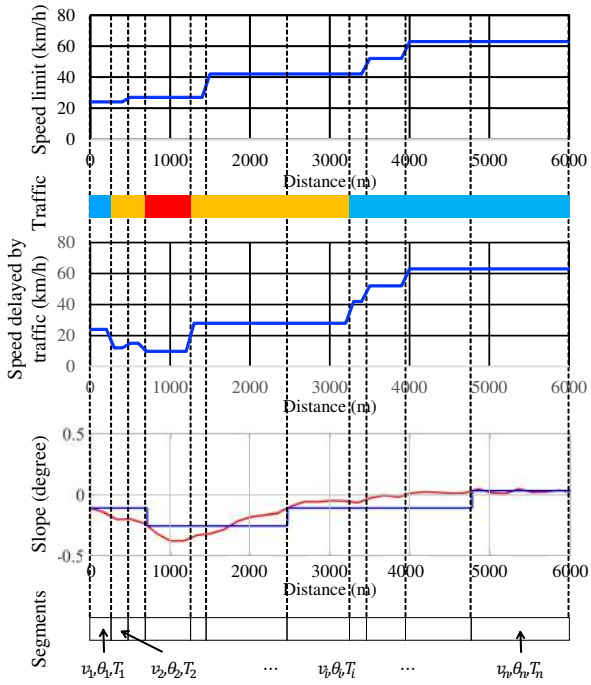

Figure 5. An example of route modeling.

change, as shown at the bottom of the plot: each segment is defined its speed v_i, road slope θ_i, and a driving time T_i.

Terrain type information was not provided in our route description but ultimately it can be easily incorporated into the model by simply specifying a different speed limit. The terrain type would rather affect the vehicle model (e.g., the friction at the tires) but this implies using a more sophisticated vehicle model than the one used in this work. In any case the modularity and flexibility of the framework allows in principle to include any detail about vehicle, route and battery models.

C. Results

1) Simulation setup: Experiments are performed on four different benchmark routes as defined in Table I. The first three are alternative and feasible routes from the same source to the same destination (benchmarks #1, #2 and #3). The latter one is selected to be reasonably longer than the EV driving range, in order to compare the proposed solution with a conventional range estimator like ADVISOR. Figure 6 shows the road slopes (in blue) and speed profiles (in red) of the four routes.

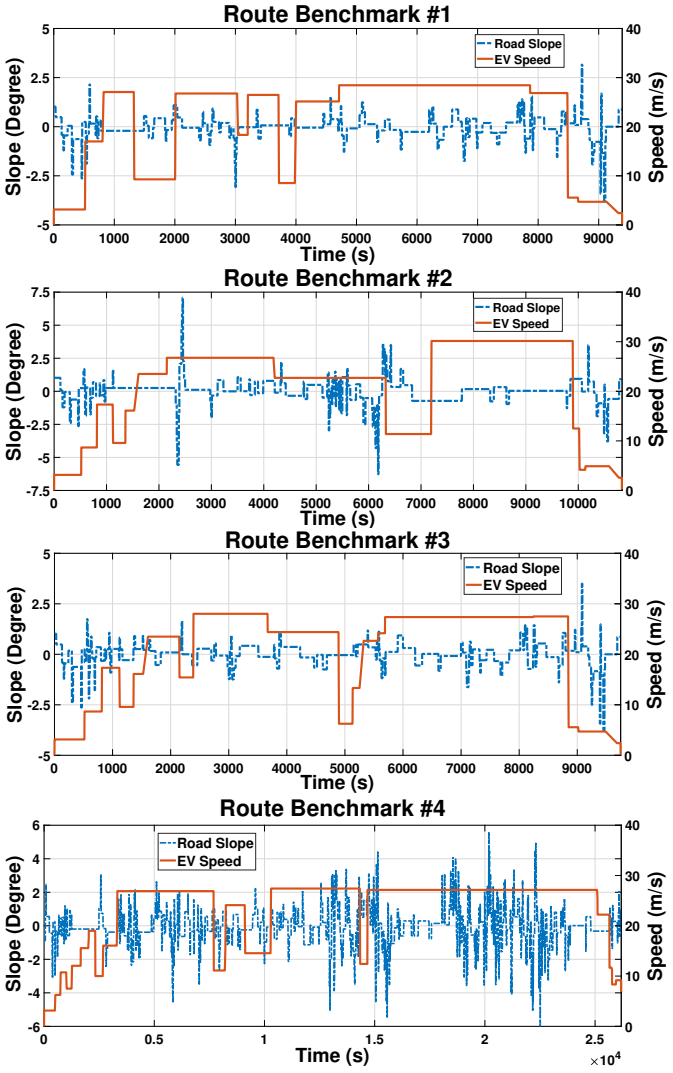

Figure 6. Slope and speed of the four benchmark routs.

Table I. ROUTE BENCHMARKS.

Route Benchmark	From	To	Distance
#1	Dusseldorf	Brussels	204 km
#2	Dusseldorf	Brussels	226 km
#3	Dusseldorf	Brussels	210 km
#4	Munich	Dusseldorf	615 km

To test the proposed solution we use the vehicle specification and experiment results of the *Tesla Model S* [37], [38]. The *Model S* has a curb weight of 2200 kg, a drag coefficient of 0.24, a maximum power of 270 kW in the range of $4300-6900$ RPM, a maximum torque of 441 Nm for engine revs less than 4300 RPM and two 3 phase AC induction electric motors in the front and rear sides. Furthermore, the *Model S* is equipped with a battery pack composed by 16 modules connected in series; each module consists of Panasonic NCR18650B 3400 mAh Lithium battery cells arranged in a 74p6s configuration. Table II summarizes the parameters of each cell, each module and the whole battery pack.

Table II. ELECTRICAL PARAMETERS OF THE BATTERY PACK.

Parameters	Cell	Module	Whole Pack
Nominal Capacity	3400 mAh	251.6 Ah	251.6 Ah
Nominal Voltage	3.6 V	21.6 V	345.6 V
Cut-off voltage	2.75 V	16.5 V	264.0 V

In order to extract the coefficients of (1), (2) and (3) we performed a number of simulations using a model implemented in ADVISOR (ADvanced VehIcle SimulatOR) [36], with the aforementioned vehicle specifications. Table III summarizes the model coefficients of the Model S. With these values, the normalized root-mean-square error between the power profile estimated by the vehicle simulator and by the model is 4.27%.

Table III. MODEL COEFFICIENTS FOR TESLA MODEL S.

α	0.098	β	9.8794	γ	0.9911	δ	0.000166
C_0	2300	C_1	11.927	C_2	4.4359	C_3	0.000321
ϵ	0.7642	ζ	2832.9				

Concerning the regenerative braking phase, we assume a charging efficiency of 20%, i.e. 20% of the kinetic energy is converted to electric energy and transferred to the battery.

2) SOC Estimation: In this first simulation we assess the importance of an accurate battery-aware SOC estimator versus a traditional one. Figure 7 shows the simulation results for route benchmark #1 assuming an initial SOC of 100%. Negative current values shown in the plot correspond to regenerative braking events. These are mostly concentrated between 8,500 seconds and the end of the route, where the road slope is negative (see Figure 6), thus making the motor torque also become negative when the EV moves at constant speed. Notice that SOC decreases lightly towards the end of the route, due to the limited power demand in that period.

The slight difference in the battery current profile determined by the two models is highlighted by the zoomed box. As expected, the battery current computed by the proposed estimator is slightly higher than that of the conventional one. Consequently, the final SOC_{end} obtained by the proposed and conventional estimators is 53.27% and 59.68%, respectively. The 6.4% overestimation by the conventional SOC estimator may not be viewed as very critical (since the final SOC is still quite large), but this is just because we started the simulation from a fully-charged condition. Table IV shows how the overestimation varies for different initial SOC values (SOC_{ini}). As expected, the discrepancy increases as SOC_{ini} decreases, since our model accounts for the decreasing effectiveness of the battery at lower SOC levels. At $SOC_{ini} = 50\%$, the initial SOC is insufficient to complete the route, despite being considered sufficient by the traditional estimator.

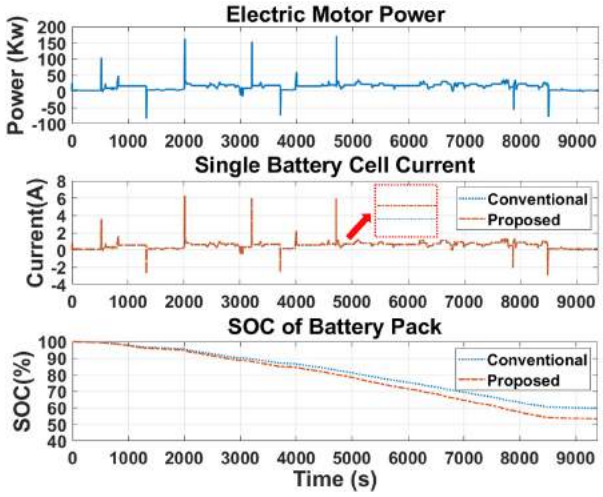

Figure 7. Difference of SOC between proposed and conventional estimator.

Table IV. SOC_{end} WITH DIFFERENT INITIAL SOC BETWEEN PROPOSED AND CONVENTIONAL ESTIMATOR.

SOC_{ini}	Proposed - SOC_{end}	Conv. - SOC_{end}	ΔSOC
100%	53.68%	59.68%	6.41%
90%	41.51%	48.43%	6.92%
80%	30.03%	37.26%	7.23%
70%	18.36%	26.04%	7.68%
60%	6.5%	14.71%	8.21%
50%	N/A	2.78%	N/A

3) Range Estimation: In this Section, we compare driving range estimates for a given battery capacity consumption. Table V shows the simulation results for route benchmark #4, and for a SOC_{ini} of 100%. The route was selected as it is the longest of the 4. The first column indicates the target SOC budget, while the second and third columns report the driving ranges computed by the two estimators for that target. These results confirm that the conventional method for driving range estimation is systematically overly-optimistic.

Table V. DRIVING RANGE ESTIMATED BY PROPOSED AND CONVENTIONAL ESTIMATOR WITH $SOC_{ini} = 100\%$.

Consumed SOC	*Range*		Δ Range
	Proposed	Conventional	[%]
60%	280.19 km	314.99 km	12.42%
50%	238.59 km	271.26 km	13.69%
40%	200.13 km	221.32 km	10.59%
30%	150.46 km	170.46 km	13.29%
20%	100.99 km	118.45 km	17.29%
10%	58.70 km	63.49 km	8.16%

Table VI shows the results of the same simulation with $SOC_{ini} = 80\%$. All ranges computed by both estimators are smaller than those with $SOC_{ini} = 100\%$, because for a given power requested by the motor, the battery provides a higher current to compensate for the decrease in battery voltage. Thus, a 10% ΔSOC from 100% to 90% is not equivalent to a ΔSOC from 80% to 70%. However, as expected, the overestimation gap increases for a smaller SOC_{ini}, again due to the state-dependent features of our battery model.

Table VI. DRIVING RANGE ESTIMATED BY PROPOSED AND CONVENTIONAL ESTIMATOR WITH $SOC_{ini} = 80\%$.

Consumed SOC	*Range*		Δ Range
	Proposed	Conventional	[%]
60%	262.83 km	297.86 km	13.33%
50%	225.68 km	260.08 km	15.24%
40%	188.28 km	212.52 km	12.87%
30%	141.65 km	163.84 km	15.67%
20%	95.25 km	114.94 km	20.67%
10%	56.69 km	62.29 km	9.88%

4) Battery-aware Economical Decision: The proposed range estimator can be used as a "plug-in" for a conventional GPS navigator. When the navigator suggests three route candidates such as route benchmarks #1, #2 and #3, it is possible to estimate both the battery consumption and the driving time for each route. The proposed battery-aware range estimator can then help drivers make economically convenient selections among the available route options.

Table VII. SOC ESTIMATION FOR DIFFERENT ROUTE CANDIDATES WITH $SOC_{ini} = 80\%$.

Route	Driving Time	SOC_{end}	ΔSOC
Benchmark #1	9,387 s	30.03%	69.97%
Benchmark #2	10,248 s	26.22%	73.78%
Benchmark #3	9,747 s	31.16%	68.84%

Table VII summarizes the simulation results for an 80% of SOC_{ini}. Route benchmark #1 is the fastest route among three route candidates. However, if we consider the energy consumption as the most important metric, the best route becomes benchmark #3, which consumes less than benchmark #1 even if it has longer driving time. In the specific example, the difference between the fastest and the least consuming route is small (a 1.13% difference in SOC) so route #1 and #3 are roughly comparable. However, the estimator can rather serve the purpose of doing a Pareto analysis by discarding route #2, which is the worst in both metrics.

VI. USE CASE 2: DELIVERY OPTIMIZATION FOR AEVS

A. AEV Model

1) Power model: Nowadays, the mostly adopted drones are quad-rotors, i.e. quadcopters. During flights, three forces act on a quadcopter.

F_W is a sum of the drone weight and payload, which pulls down the drone due to the force of gravity. F_{DH} and F_{DV} are forces for dragging in horizontal (F_{DH}) and vertical directions, which oppose movements of the drone in horizontal and vertical directions, respectively. F_T represents the thrust produced by rotating propellers of the drone and opposes the weight and drag to sustain the height and speed of the drone. Weight with a mass of the drone and payload (w_d, w_p) and drag with horizontal and vertical speeds (v_h, v_v) are modeled by (4):

$$F_W = (w_d + w_p)g, F_{DV} = \frac{1}{2}\rho A_t C_d v_v^2, F_{DH} = \frac{1}{2}\rho A_f C_d v_h^2 \quad (4)$$

where g is gravity; A_f and A_t are cross sectional areas in horizontal and vertical directions; C_d is drag coefficient; ρ is air density. The required thrust to oppose weight and drag is given by (5):

$$F_{T,v} = F_W + F_{DV} \text{ and } F_{T,h} = \sqrt{F_W^2 + F_{DH}^2}. \quad (5)$$

Thrust in terms of motor angular speed is modeled by:

$$F_T = 0.5\rho A_p C_t (\omega r)^2 \quad (6)$$

where A_p is the disk area of propellers; C_t is a thrust coefficient; ω is angular speed of motors; r is radius of propellers. Thrust coefficient obtained with several experiments ranges from 0.01 to 0.05 [39]. We can calculate (i) the required thrust for a given drone flight (vertical and horizontal velocities) and payload by solving (4) and (5) and (ii) the required angular speed to obtain the thrust from (6).

These basic equations of forces allow us to derive the required angular speed to sustain the drone (i) at a given height and flying at a constant horizontal speed v_h (ω_h), and (ii) to sustain a constant vertical speed v_v (ω_v), yielding the following equations:

$$\omega_h = \frac{(4(w_d + w_p)^2 g^2 + \rho^2 A_f^2 C_d^2 v_h^4)^{1/4}}{(r^2 \rho A_p C_t)^{1/2}} = f_h(w_p,\ v_h), \quad (7)$$

$$\omega_v = \frac{(2(w_d + w_p) g + \rho A_t C_d v_v^2)^{1/2}}{(r^2 \rho A_p C_t)^{1/2}} = f_v(w_p,\ v_v). \quad (8)$$

We refer to the drone flight measurement data from [40] where motor current, voltage and angular speed over the drone flight time are specified. The motor current and voltage by angular speed include the efficiency of the motor and motor controller. This measurement data was obtained with Parrot AR. Drone 2.0, which is 420 g without payload, and the maximum motor angular speed is 500 rad/s. We fitted the measurement to obtain a polynomial motor power consumption model as

$$P = g(\omega) \approx 2.26{\cdot}10^{-7}\omega^3 + 3.87{\cdot}10^{-5}\omega^2 + 5.14{\cdot}10^{-3}\omega + 2.62. \quad (9)$$

By plugging the expressions of (7)-(8) to (9), we can obtain motor power consumption as a function of payload and speed for the flight both in horizontal direction (P_h) and vertical direction (P_v) as

$$P_h(w_p, v_h) \approx g(f_h(w_p, v_h)) \quad P_v(w_p, v_v) \approx g(f_v(w_p, v_v)). \quad (10)$$

B. Route Model

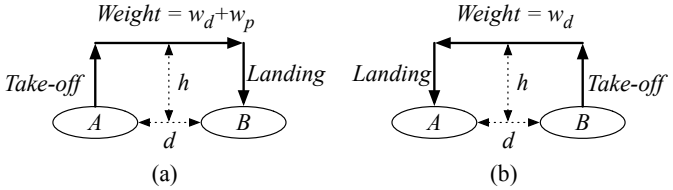

Figure 8. A drone flight model (a) going to place B with a payload and (b) returning to place A without payload.

Unlike terrestrial EV in Section V, drones flight speed is not limited by speed limit and traffic. Thus, instead of modeling flight speed by segment, we can optimize the flight speed until it arrives at the destination. Figure 8 shows simple drone flight model, which consists of (i) take-off from a place A with constant vertical speed v_v to the height h, (ii) flight horizontally during distance d with constant speed v_h and (iii) landing with the same vertical speed on a place B. The drone returns to the place A after taking down a package. The overall energy consumption for one delivery is obtained by

$$E \approx P_v(w_p, v_v)\frac{h}{v_v} + P_h(w_p, v_h)\frac{d}{v_h} + P_v(w_p, -v_v)\frac{h}{|-v_v|} + P_v(0, v_v)\frac{h}{v_v} + P_h(0, v_h)\frac{d}{v_h} + P_v(0, -v_v)\frac{h}{|-v_v|}. \quad (11)$$

We assume that the vertical speed for take-off and landing is 3 m/s, which is the maximum vertical speed of AR.Drone 2.0. The height of the drone during horizontal flight is 40 m.

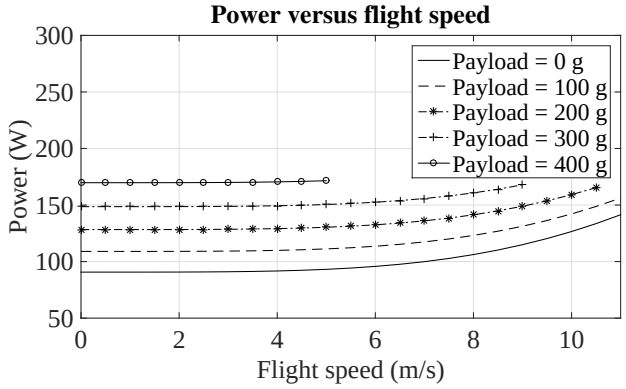

Figure 9. Drone motor power vs. flight speed and payload.

Figure 9 shows the power consumption as a function of horizontal speed and payload. Zero flight speed coincides with hovering power. The power consumption is almost constant at slow flight speeds because the drag is relatively small compared with weight.

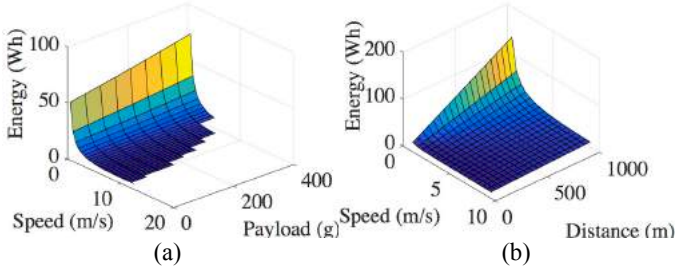

Figure 10. Energy curve (a) when the distance is 500 m and (b) when the payload is 300 g with 100% battery SOC.

Energy for a given delivery task (11) is shown in Figure 10. It is a 3-variable function of weight, delivery distance, and flight speed, which is displayed in the figure as two different projections. In general, the maximum horizontal speed decreases with payload because the maximum thrust opposing the weight

and drag is bounded by the maximum motor angular speed. Moreover, there is an energy-optimal horizontal speed for a given delivery task. Too slow horizontal speed causes huge energy consumption because the drone consumes most energy to maintain the altitude during the long delivery time. On the other hands, too fast horizontal speed increases drag by the air, which is proportional to the square of the horizontal speed. The energy-optimal speed should be increased as the payload increases in order to reduce the delivery time.

C. Adding Battery Awareness

Figures 9–10 are indeed referring to the power and energy *of the drone hardware* and their relation to the relevant quantities (weight, distance, and delivery time via the flight speed). For an useful evaluation of the actual energy assessment and the feasibility of a given delivery task, however, we need to map the relations descried in Figure 10 onto *battery energy*. This require accounting for two issues: *Battery sensitivity to load currents* and *non-ideal conversion efficiency*.

1) Current-Dependent Battery Efficiency: The fundamental effect to be taken into account is the *rated capacity*. Incorporating this effect into our model requires conceptually to project the "energy" dimension on the y-axis of Figure 10 onto the "battery energy" one. As energy is obtained as the product of power and flight time, mapping drone energy to battery energy cannot be done "statically" (i.e., by a direct conversion), but requires the battery ECM described in Section IV. Consequently, our power model relies on an offline pre-characterization phase described in Section VI-C2.

2) Construction of the Power Model: The power model consists of a 5-dimensional table that is built offline according to the flow described in Algorithm 1. The table stores all possible values of battery SOC drop in response to a given delivery task.

Algorithm 1 Offline Model Characterization

1: **for** $\forall$ weight $w_i \in [0, w_{max}]$ **do**
2: **for** $\forall$ *speed* $v_i \in [v_{min}, v_{max}]$ **do**
3: **for** $\forall$ distance $d_i \in [d_{min}, d_{max}]$ **do**
4: calculate $P_{|w=wi,d=di,v=vi}(t)$ //see Figure 8
5: calculate $I_{batt}(t) = P_{|w=wi,d=di,v=vi}(t)/V_{batt}(t)$
6: **for** $\forall$ SOC level $SOC_i \in [10, 100]$ **do**
7: calculate ΔSOC_i by applying $I_{batt}(t)$ to the
8: battery model and store it in $T[w_i, d_i, v_i, SOC_i]$

We have to build the battery energy by actually building the *power profile* of a given delivery task (i.e., as in Figure 8). In Line 1–4 we build all possible power profiles for each combination of valid weight, distance, and horizontal speed; this yields a waveform $P(t)_{|w=w_i,d=d_i,v=v_i}$[2]. This includes take-off, the first leg to the target, landing, take-off, second leg to the base, and landing.

Since $P(t)$ is the motor power profile, we need to translate it into battery power; this is done by dividing the motor power by the current battery voltage (Line 5), which yields a current waveform $I_{batt}(t)$.

[2]As already discussed, we assume a fixed vertical speed of 3 m/s

We then apply (Line 7) this current profile to a battery simulation model described in Section IV; the model allows to track the decrease of SOC of the battery for a given current profile. The amount of consumed SOC is then stored into the table **T**, which represents the actual model.

T is a 5-dimensional table that returns the decrease of battery SOC resulting from a drone delivery over a distance d_i, carrying a payload w_i, at a speed v_i, and for a battery having SOC level SOC_i at the beginning of the delivery.

The computational cost of build the model is obviously determined by the discretization interval for the various quantities. For building function $E()$, the cost is $O(|W| \cdot |D| \cdot |V| \cdot |S|)$, where $|W|, |D|, |V|$ and $|S|$) are the number of discretized levels of weights, distances, speeds, and SOC, respectively. In our case we have $|W| = 4$ (payload = 100 to 400 g, step = 100 g), $|D| = 10$ (distance = 100 to 1000 m, step = 100 m), $|V| = 11$ (speeds = 1 to 11 m/s, step = 1 m/s), and $|S| = 10$ (SOC = 10% to 100%, step = 10%); the calculation involves therefore 4400 invocations of the battery model of [32].

3) Usage of the Power Model: Given **T**, the simulation of a sequence of delivery tasks is relatively straightforward. The only computation involved is the calculation of the optimal flight speed.

Given a task τ_a with payload w_a and delivery distance d_a, and the current battery SOC SOC_a (100% for the first task), we extract the projection $\mathbf{T}(v)_{|w=w_a,d=d_a,SOC=SOC_a}$ of **T** describing the the ΔSOC corresponding to the triple $w = w_a, d = d_a, SOC = SOC_a$, and where speed is left as the only free variable. On this single variable function, we then simply search of the speed value $v_{opt,a}$ that yields the smallest $\Delta SOC_a = min_v \mathbf{T}(v)_{|w=w_a,d=d_a,SOC=SOC_a}$; this will be the optimal battery-aware flight speed. The next task τ_b will be executed assuming an initial SOC $\text{SOC}_b = \text{SOC}_a - \Delta\text{SOC}_a$. The optimal speed v_b and the minimum ΔSOC_b are thus obtained as describe above, and the process is repeated for all tasks in the task set.

D. Simulation Results

1) Simulation Setup: We selected the *Parrot AR.Drone 2.0* device, since there are comprehensive measurement data available in [40], which allows us to build the drone power consumption model 9. Concerning the battery, we used the *Ultimate PX-04 LIPO Battery*, which has 1,000 mA rated capacity, 11.1 V nominal voltage and 9.0 V cut-off voltage. Then we modeled a battery pack of 5,000 mAh rated capacity at 11.1 V nominal voltage followed the method described in Section IV, and assumed a constant converter efficiency of 90%.

2) Delivery Task Battery-aware Scheduling: In order to show how the proposed battery-aware energy model can be applied in a general framework involving a set of delivery tasks, we formulated a couple of scenarios related to the scheduling of a set of drone deliveries. In this context, a number n of delivery tasks $\{\tau_1, ...\tau_n\}$ have to be carried out by a given drone. Each delivery $\tau_i = (w_i, d_i)$ is characterized by a payload weight w_i and a distance d_i from the base station to the delivery target. We assumed that only one package is delivered for each task.

3) Comparison of Different Scheduling: In this experiment, we generated two sets of delivery tasks with different payloads and distances, whose specific values are shown in Table VIII. Among all possible deliver orders from six independent tasks,

Table VIII. DELIVERY TASKS FOR SET A AND SET B.

	Set A		Set B	
Task	W (g)	D (m)	W (g)	D (m)
1	100	100	300	100
2	200	100	400	100
3	100	200	400	200
4	100	300	400	300
5	200	500	200	500
6	400	900	100	900

we report the best and worst cases. *Best case* means that all the tasks are delivered with the minimum energy and, therefore, there is still available capacity in the battery, whereas *worst case* means that the drone cannot finish all the delivery tasks because the battery is fully depleted. In terms of set A, we found that the best scheduling is $6 \rightarrow 5 \rightarrow 2 \rightarrow 4 \rightarrow 3 \rightarrow 1$, while the worst scheduling is the mirrored one.

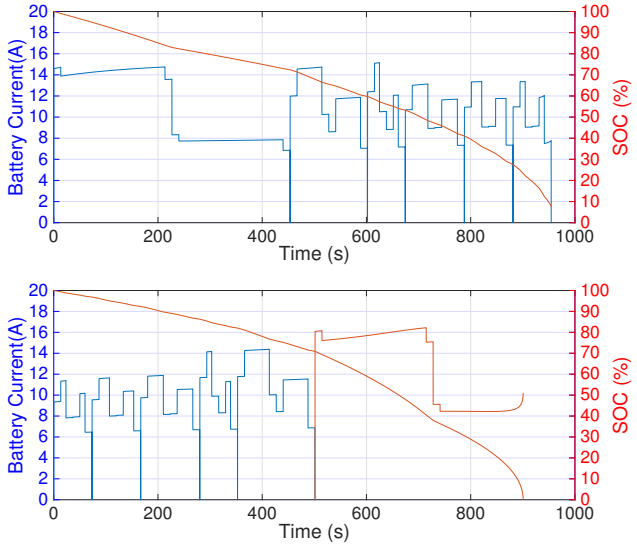

Figure 11. Best and worst scheduling of delivery task set A.

Figure 11 shows the battery current and SOC during delivering all the tasks of set A. The upper sub-figure corresponds to the best scheduling case: the battery SOC is 7.81% after delivering all the tasks. On the other hand, in the worst scheduling case, they cannot be all accomplished before the battery is exhausted, as shown in the bottom sub-figure. Notice that, at constant power, the discharge current increases dramatically at the ending phase because the battery voltage decreases evidently at low SOC. This is determined by the non-linear characteristics of the battery behavior. It is also the reason why the current provided by battery for task F in the worst scheduling case is slightly higher than the one in the best scheduling case. Concerning set B, we got a similar result.

Notice that the best scheduling policy always starts with the task having the heaviest payload and longest distance. In fact, since the battery is more efficient in *serving* larger current requests when fully charged, an effective scheduling policy would be *heaviest-longest-first*.

4) Using the Model as an Accurate Predictor: In order to analyze how many tasks can be really accomplished, we used the scheduling policy *heaviest-and-longest-first* on the task set described in Table IX, and then we compared the results of the proposed energy model against the classical model.

Table IX. DELIVERY TASKS WITH VARIOUS PAYLOADS AND DISTANCES.

Task	W (g)	D (m)	Task	W (g)	D (m)
1	300	100	4	300	400
2	100	200	5	400	600
3	400	300	6	200	900

The optimal scheduling is $5 \rightarrow 3 \rightarrow 4 \rightarrow 1 \rightarrow 6 \rightarrow 2$. Figure 12 shows that the residual battery SOC is estimated at 15% after delivering all the tasks when considering the classic model, whereas the battery is fully discharged during the delivery of the last task using a battery-aware model. Therefore, the proposed model can suggest the right decision weather or not to start the last delivery by considering *effective* capacity of the battery accurately.

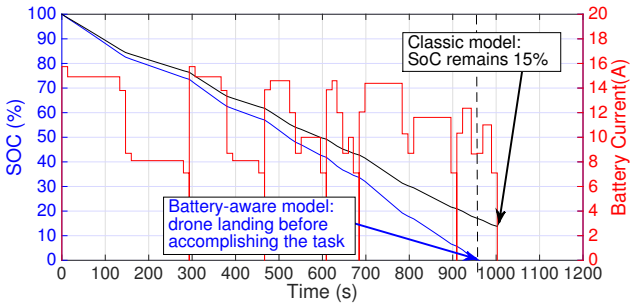

Figure 12. Comparison of the battery-aware model and classic model.

VII. CONCLUSION

For electric vehicles, a careful planning of the driving and/or flying range is essential to guarantee the service without charge depletion during operation. In this work, we proposed a framework that has generality and modularity as its key features: by decoupling the information about (i) the vehicle, (ii) the route, and (iii) the battery it is possible to easily model different scenarios. We demonstrated these features by proposing two use cases, one more traditionally oriented towards simulation consisting of a range estimation, and a second one that solves an optimization problem, namely the optima flying speed of for a set of AEV delivery tasks.

Our framework can be extended in several ways that will be the subject of future work. One direction would be to extend the route model to include route conditions both in terms of environmental conditions (humidity, weather) and even terrain types (for TEVs only). These extensions will clearly impact also the vehicle models, which should become sensitive to these quantities through additional dependencies on new variables.

Another possible extensions concerns a more elaborated weight model for TEVs and the relative dependence of the vehicle model on weight, as already considered for AEVs in the second use case. Again, this should be reflected by the TEV model, which in the current version considers only a static weight.

REFERENCES

[1] K. Li and K. J. Tseng, "Energy efficiency of lithium-ion battery used as energy storage devices in micro-grid," in *41st Annual Conference of the IEEE Industrial Electronics Society (IECON)*. IEEE, 2015, pp. 005 235–005 240.

[2] D. Floreano and R. J. Wood, "Science, technology and the future of small autonomous drones," *Nature*, vol. 521, no. 7553, p. 460, 2015.

[3] W. Xiaoqin, L. Hu, R. Qiaolin, W. Yan, and X. Wei, "Overview of the development and related research of electric vehicles," in *2017 2nd International Conference on Power and Renewable Energy (ICPRE)*, Sep. 2017, pp. 814–818.

[4] S. Chen, D. F. Laefer, and E. Mangina, "State of technology review of civilian UAVs," *Recent Patents on Engineering*, vol. 10, no. 3, pp. 160–174, 2016.

[5] R. Zhang, B. Xia, B. Li, L. Cao, Y. Lai, W. Zheng, H. Wang, and W. Wang, "State of the art of lithium-ion battery SOC estimation for electrical vehicles." *Energies (19961073)*, vol. 11, no. 7, pp. 1–36, 2018.

[6] Y. Wang, C. Feng, G. Liu, H. Fu, S. Xue, L. Lu, J. Hua, and M. Ouyang, "Research on driving range estimation for EVs based on corrected battery model," in *SAE 2015 World Congress & Exhibition*, 2015.

[7] Y.-W. Wang, C.-C. Lin, and T.-J. Lee, "Electric vehicle tour planning," *Transportation Research Part D: Transport and Environment*, vol. 63, pp. 121–136, 2018.

[8] S. M. Rezvanizanian, Y. Huang, J. Chuan, and J. Lee, "A mobility performance assessment on plug-in EV battery," *Int. J. Progn. Health Management*, vol. 3, no. 2, pp. 1–8, 2012.

[9] J. Wang, I. Besselink, and H. Nijmeijer, "Battery electric vehicle energy consumption prediction for a trip based on route information," *Proceedings of the Institution of Mechanical Engineers, Part D: Journal of Automobile Engineering*, vol. 232, no. 11, pp. 1528–1542, 2017.

[10] J. Yang, L. Chou, and Y. Chang, "Electric-vehicle navigation system based on power consumption," *IEEE Transactions on Vehicular Technology*, vol. 65, no. 8, pp. 5930–5943, Aug 2016.

[11] J. Hong, S. Park, and N. Chang, "Accurate remaining range estimation for electric vehicles," in *2016 21st Asia and South Pacific Design Automation Conference (ASP-DAC)*. IEEE, 2016, pp. 781–786.

[12] S. Kachroudi, M. Grossard, and N. Abroug, "Predictive driving guidance of full electric vehicles using particle swarm optimization," *IEEE Trans. on Vehicular Technology*, vol. 61, no. 9, pp. 3909–3919, 2012.

[13] K. Vatanparvar, J. Wan, and M. A. Al Faruque, "Battery-aware energy-optimal electric vehicle driving management," in *International Symposium on Low Power Design (ISLPED)*, 2015, pp. 353–358.

[14] L. Lu, X. Han, J. Li, J. Hua, and M. Ouyang, "A review on the key issues for lithium-ion battery management in electric vehicles," *Journal of Power Sources*, vol. 226, pp. 272–288, 2013.

[15] M. A. Hannan, M. Lipu, A. Hussain, and A. Mohamed, "A review of lithium-ion battery state of charge estimation and management system in ev applications: Challenges and recommendations," *Renewable and Sustainable Energy Reviews*, vol. 78, pp. 834–854, 2017.

[16] Y. Zheng, M. Ouyang, X. Han, L. Lu, and J. Li, "Investigating the error sources of the online state of charge estimation methods for lithium-ion batteries in electric vehicles," *Journal of Power Sources*, vol. 377, pp. 161–188, 2018.

[17] Y. Chen, D. J. Pagliari, E. Macii, and M. Poncino, "Battery-aware design exploration of scheduling policies for multi-sensor devices," in *2018 ACM/IEEE 28th Great Lakes symposium on VLSI (GLSVLSI)*. ACM/IEEE, 2018, pp. 201–206.

[18] F. Morbidi, R. Cano, and D. Lara, "Minimum-Energy Path Generation for a Quadrotor UAV," in *2016 IEEE International Conference on Robotics and Automation (ICRA)*, 2016, pp. 1492–1498.

[19] C. Di Franco and G. Buttazzo, "Energy-aware coverage path planning of UAVs," in *2015 IEEE International Conference on Autonomous Robot Systems and Competitions (ICARSC)*, 2015, pp. 111–117.

[20] J. Modares, F. Ghanei, N. Mastronarde, and K. Dantu, "UB-ANC Planner: Energy Efficient Coverage Path Planning with Multiple Drones," in *2017 IEEE International Conference on Robotics and Automation (ICRA)*, 2017, pp. 6182–6189.

[21] K. Chang, P. Rammos, S. A. Wilkerson, M. Bundy, and S. Andrew Gadsden, "LiPo battery energy studies for improved flight performance of unmanned aerial systems," in *Unmanned Systems Technology XVIII.*, 2016, p. 98370W.

[22] K. Goss, R. Musmeci, and S. Silvestri, "Realistic Models for Characterizing the Performance of Unmanned Aerial Vehicles," in *26th International Conference on Computer Communication and Networks (ICCCN)*, 2017, pp. 1–9.

[23] A. Abdilla, A. Richards, and S. Burrow, "Power and endurance modelling of battery-powered rotorcraft," in *2015 IEEE/RSJ International Conference on Intelligent Robots and Systems*, September 2015, pp. 675–680.

[24] M. Podhradský, C. Coopmans, and A. Jensen, "Battery state-of-charge based altitude controller for small, low cost multirotor unmanned aerial vehicles," *Journal of Intelligent & Robotic Systems*, vol. 74, no. 1-2, pp. 193–207, 2014.

[25] M. Chen and G. Rincón-Mora, "Accurate electrical battery model capable of predicting runtime and IV performance," *IEEE Transactions on Energy Conversion*, vol. 21, no. 2, pp. 504–511, 2006.

[26] K. Dorling, J. Heinrichs, G. G. Messier, and S. Magierowski, "Vehicle routing problems for drone delivery," *IEEE Transactions on Systems, Man, and Cybernetics: Systems*, vol. 47, no. 1, pp. 70–85, January 2017.

[27] S. Poikonen, X. Wang, and B. Golden, "The vehicle routing problem with drones: Extended models and connections," *Networks*, vol. 70, no. 1, pp. 34–43, 2017.

[28] L. Lee, "Optimization of a modular drone delivery system," in *2017 Annual IEEE International Systems Conference (SysCon)*, April 2017, pp. 1–8.

[29] S. Park, L. Zhang, and S. Chakraborty, "Battery assignment and scheduling for drone delivery businesses," in *2017 IEEE/ACM International Symposium on Low Power Electronics and Design (ISLPED)*, 2017.

[30] D. Aleksandrov and I. Penkov, "Energy consumption of mini UAV helicopters with different number of rotors," in *11th International Symposium Topical Problems in the Field of Electrical and Power Engineering*, 2012, pp. 259–262.

[31] Google Maps, [Online] Available: https://www.google.com/maps.

[32] Y. Chen, E. Macii, and M. Poncino, "A circuit-equivalent battery model accounting for the dependency on load frequency," in *Proceedings of the Conference on Design, Automation & Test in Europe*. European Design and Automation Association, 2017, pp. 1177–1182.

[33] L. Benini, G. Castelli, A. Macii, E. Macii, M. Poncino, and R. Scarsi, "Discrete-time battery models for system-level low-power design," *IEEE Transactions on VLSI Systems*, vol. 9, no. 5, pp. 630–640, 2001.

[34] A. Bocca, A. Macii, E. Macii, and M. Poncino, "Composable battery model templates based on manufacturers' data," *IEEE Design & Test*, vol. 35, no. 3, pp. 66–72, 2018.

[35] Y. Chen, E. Macii, and M. Poncino, "Frequency domain characterization of batteries for the design of energy storage subsystems," in *2016 IFIP/IEEE International Conference on Very Large Scale Integration (VLSI-SoC)*. IEEE, 2016, pp. 1–6.

[36] T. Markel, A. Brooker, T. Hendricks, V. Johnson, and K. Kelly, "Advisor: a systems analysis tool for advanced vehicle modeling," *Journal of Power Sources*, 2002.

[37] "Tesla Model S Specs," Tesla Website, [Online] Available: https://www.tesla.com/models.

[38] "Tesla Model S Efficiency and Range," Tesla Official Website, [Online] Available: https://www.tesla.com/blog/model-s-efficiency-and-range.

[39] S. Newman, *The foundations of helicopter flight*. Halsted Press, 1994. [Online]. Available: https://books.google.it/books?id=3LhTAAAAMAAJ

[40] N. L. M. Jeurgens, "Implementing a Simulink controller in an AR.Drone 2.0," DC 2016.005, Eindhoven University of Technology, January 2016.

Donkyu Baek (M'15) is a postdoctoral research fellow in the Department of Control and Computer Engineering (DAUIN) at Politecnico di Torino, Italy since 2018. He received Ph.D. degree in Electrical Engineering at Korea Advanced Institute of Science and Technology (KAIST), Korea, in 2017. His current research interests include the battery-aware delivery electric vehicle and drone range estimation and route planning. He is a Member of the IEEE.

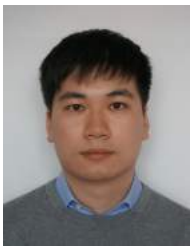

Yukai Chen (M'18) received the M.Sc. degree in computer engineering and the Ph.D. degree in computer and control engineering from the Politecnico di Torino, Turin, Italy, in 2014 and 2018, where he is currently a Postdoctoral Research Fellow. His current research interest includes computer-aided design for integrated circuits and cyber physical energy systems, with particular emphasis on the modeling and simulation of extra-functional properties.

Alberto Bocca (M'16) joined the EDA Group at Politecnico di Torino, Turin, Italy, where he is currently a Research Assistant. His interests focus mainly on low-power VLSI design, with a particular emphasis on CAD solutions for clock tree optimization and leakage-aware design, electrical energy storage devices in mobile systems, and photovoltaic applications. He received both the BS and MS degrees in electronic engineering from Politecnico di Torino. He is a Member of the IEEE.

Lorenzo Bottaccioli (M'15) is Assistant Professor at the Energy Center Lab of Politecnico di Torino (Italy). In 2018 received the PhD, cum laude, in Computer Engineering at Politecnico di Torino. His main research interests concern Smart Energy, Smart City and Smart Communities with focus on software solutions i) for planning, analysing and optimising smart energy system and ii) for spatial representation of energy information. He is a Member of the IEEE.

Santa Di Cataldo (M'07) is Assistant Professor (Tenure Track) at the Dept. of Control and Computer Engineering of Politecnico di Torino (Italy). She received a PhD in Computer and Systems Engineering from the same university in 2011. Her main research interests are Artificial Intelligence, Machine Learning and Image Processing, with special regards to medical and smart manufacturing applications. She is a Member of the IEEE.

Valentina Gatteschi (M'19) is an Assistant Professor with time contract at the Department of Control and Computer Engineering at Politecnico di Torino, Italy. She received the PhD degree in Computer Engineering from Politecnico di Torino, Italy in 2013. Her main interests are Natural Language Processing, Human-Computer Interaction and Blockchain technology. She is a Member of the IEEE, and she participates to the IEEE Blockchain Initiative Subcommittee on Education. Contact her at valentina.gatteschi@polito.it (website: staff.polito.it/valentina.gatteschi).

Daniele Jahier Pagliari (M'15) received the M.Sc. and Ph.D. degrees in Computer Engineering from Politecnico di Torino, Italy, in 2014 and 2018 respectively. He is currently Assistant Professor at the same institution. His main research interests focus on computer-aided design of digital systems, with particular emphasis on low-power optimization and approximate computing.

Edoardo Patti (M'16) is Assistant Professor at Politecnico di Torino. He received both M.Sc. and Ph.D. degrees in Computer Engineering at Politecnico di Torino in 2010 and 2014, respectively. His research interests concern: i) Ubiquitous Computing and Internet of Things; ii) Smart Systems, Cities and Mobility; iii) Software architectures with particular emphasis on infrastructure for Ambient Intelligence; iv) Software solutions for simulating and optimising energy systems; v) Software solutions for energy data visualisation to increase user awareness.

Gianvito Urgese (M'13) is Postdoc at the Dept. of Control and Computer Engineering of Politecnico di Torino (Italy) where he received a PhD in Computer and Systems Engineering in 2016. His main research interests are Neuromorphic Engineering, Parallel and Heterogeneous Architectures, and Algorithm Optimisation focused on Bioinformatics and Embedded-Systems domains. He is a Member of the IEEE.

Naehyuck Chang (F'12) is a Full Professor at the School of Electrical Engineering, Korea Advanced Institute of Science and Technology (KAIST). His current research interests include low-power embedded systems and design automation of things, such as systematic design and optimization of energy storage systems and electric vehicles. Dr. Chang is an ACM Fellow and an IEEE Fellow for the contribution to low-power design.

Alberto Macii (SM'07) is currently a Full Professor of Computer Engineering with the Politecnico di Torino, Turin, Italy. He holds Laurea and PhD degrees in computer engineering from the Politecnico di Torino. His research interests are in the design of electronic digital circuits and systems, with a particular emphasis on low-power consumption aspects. He is a Senior Member of the IEEE. email address: alberto.macii@polito.it

Enrico Macii (F'05) is a Full Professor of Computer Engineering with the Politecnico di Torino, Torino, Italy. He holds a Laurea degree in electrical engineering from the Politecnico di Torino, a Laurea degree in computer science from the Universit di Torino, Turin, and a PhD degree in computer engineering from the Politecnico di Torino. His research interests are in the design of electronic digital circuits and systems, with a particular emphasis on low-power consumption aspects. He is a Fellow of the IEEE. email address: enrico.macii@polito.it

Paolo Montuschi (M'90-SM'07-F'14) (paolo.montuschi@polito.it) is a Full professor with the Department of Control and Computer Engineering and a Member of the Board of Governors at Politecnico di Torino, Italy. His research interests include computer arithmetic, computer graphics, and intelligent systems. He is an IEEE Fellow, and a life member of the International Academy of Sciences of Turin, and of Eta Kappa Nu, the Honor Society of IEEE. More information at http://staff.polito.it/paolo.montuschi.

Massimo Poncino (SM'12-F'18) is a Full Professor of Computer Engineering with the Politecnico di Torino, Torino, Italy. His current research interests include several aspects of design automation of digital systems, with emphasis on the modeling and optimization of energy-efficient systems. He received a PhD in computer engineering and a Dr.Eng. in electrical engineering from Politecnico di Torino. He is a Fellow of the IEEE.